GSA DATA REPOSITORY 2020118

"Integrated geophysical characterization of crustal domains in the eastern Black Sea"

Vanessa Monteleone[1, 2], Tim A. Minshull[1], and Hector Marin-Moreno[2]

[1] School of Ocean and Earth Science, University of Southampton, Waterfront Campus, European Way, Southampton, SO14 3ZH, United Kingdom

(v.monteleone@soton.ac.uk; tmin@noc.soton.ac.uk).

[2]National Oceanography Centre, University of Southampton Waterfront Campus, European Way, Southampton, SO14 3ZH, United Kingdom

(hector.marin.moreno@noc.ac.uk).

Content of this file

DETAILS OF METHODS

Seismic Data

Twelve post-stack time-migrated seismic reflection profiles are used in this study (Fig. DR1, DR2). The dataset was acquired in 2011 by Geology Without Limits (GWL) and ION GXT. Table DR1 provides information about the acquisition parameters and the processing steps carried out by GWL.

2011 Long-Offset - Acquisition parameters					
Source		Streamer		Recorder	
Array volume	5680 cu.in	Length	10200 m	Sampling rate	2.0 ms
shot interval	50 m	Channels	860	Record length	18 sec
Depth	8 m ± 0.5 m	Receiver spacing	12.5 m	Filters LC	3 Hz
Pressure	2000 PSI	Depth	9 m ± 0.5 m	Filters HC	200 Hz
		Offset min	149.5 m		
		Offset max	10500 m		

Processing steps
segy input and geometry application
Spherical divergence correction
Velocity analysis
Predictive deconvolution 8 ms, 240 ms, wn 1%
Radon demultiple
Amplitude balancing
NMO muting and stacking
Kirchhoff migration
BP filter 4-8-100-120 Hz
Coherent filtering
Amplitude balancing

Table DR1. Top) Summary of the 2D long-offset seismic reflection profiles acquisition parameters; bottom) GWL processing steps used to generate the post-stack time migrated profiles.

We converted time migrated profiles into depth using interval velocities derived from GWL stacking velocities, combined with wide-angle tomographic velocities from Shillington et al. (2009). A comparison between the two velocity trends shows that velocities above basement reflection are similar, but stacking velocities are widespread across the study region and they better follow geological variations across seismic sections. Below basement, stacking velocities have a single, low-velocity, and linearly increasing trend, whereas wide-angle data show faster velocity trends with more realistic gradient changes, making them more reliable at depths below basement.

Velocity model creation was performed on Petrel 2015 software. Seismically interpreted horizons, corresponding to main acoustic impedance contrasts, were used to define a four-layer model. Each layer was defined by a V0 velocity (top layer velocity) representing the averaged stacking/wide-angle velocities along the layer-bounding horizons. A mean velocity gradient was estimated between top and bottom layer velocities and applied to the model. Further information about the velocity model creation, and time-depth conversion steps is given by Monteleone et al. (2019).

Magnetic Anomaly Data

We used the Earth Magnetic Anomaly Grid (EMAG2-v3, www.NOAA.gov) over the EBSB region (Fig. DR2), which is specified as a 2-arc-minute resolution grid of the total intensity magnetic anomaly at an altitude of 4 km above mean sea level, and it is compiled from satellite, marine, aero-magnetic and ground magnetic surveys (Maus et al., 2009; Meyer et al., 2017).

A reduction-to-pole (RTP) transform was applied to the magnetic anomaly grid. RTP reduces the magnetic anomalies to the pole and corrects for variations in inclination and declination over the

study area (Baranov, 1957). Declination, inclination, and magnitude of the modern Earth's magnetic field were taken according to IGRF field (Thébault et al., 2015). RTP was applied to the total intensity magnetic map using a declination of 6° and an inclination of 61° at the center of the EBSB.

Magnetic Anomaly Modelling

Inverse modeling of magnetic anomalies is generally used when well-defined constraints are available (e.g., Parker and Huestis, 1974; Russell and Whitmarsh, 2003). Such inverse models result in calculated anomalies that match closely those observed, including those resulting from 3D effects, and inverse models of 2D profiles will not normally match at profile crossings. To avoid over-fitting the data, and to ensure that models of crossing profiles are consistent with each other, we use a forward modeling approach. Due to the inherent non-uniqueness of such forward models, we kept them simple and made no attempt to produce perfect fits of the observed anomalies. Such a forward modeling approach has been used commonly along continental margins elsewhere (e.g., Bronner et al., 2011; Rippington et al., 2015).

Forward modelling was undertaken using Geosoft software, Oasis Montaj V9.4 along the seismic profiles. These models were built from SEG-Y files of the seismic data and modelled against the gridded potential field data sampled along the corresponding sections. Our 2D models assume that there are no variations perpendicular to the profiles. However, because the observed anomaly results from 3D effects, we include the anomaly variations within about 15 km either side of the magnetic profiles (grey bands; Fig. DR2-DR7). The choice of a 15 km range is due to the high geological variability perpendicular to the magnetic profiles. Ranges > 15 km would

85 introduce anomaly trends from different crustal structures domains, especially along the NW-SE-
86 trending profiles.
87 Magnetic anomaly profiles were extracted from the RTP EMAG2-v3 grid, and used to
88 complement seismic sections (Fig. DR2-DR7). Modelling was constrained by the top basement
89 reflection interpreted from seismic data. Because the sedimentary cover has a very low
90 magnetization in the Black Sea region (e.g., Ross, 1978), modelling was done considering the
91 upper boundary of the magnetized layer to coincide with the top basement. Crustal layers and
92 magmatic bodies modelled along the top basement were assumed to have attained their
93 magnetization during the Late Cretaceous and/or Early Cenozoic (e.g., Nikishin et al., 2015) at
94 approximately their present latitude, so no paleo-latitude correction was applied in this study. No
95 susceptibility data are available for the central EBSB, and little information is available from
96 values of magnetic susceptibility of adjacent onshore samples (e.g., Rangin et al., 2002;
97 Hippolyte et al., 2010). Thus, we were guided by average values of magnetization estimated for
98 different type of magnetized rocks (e.g., Hunt et al., 1995).
99 We started with the simplest possible model characterized by a non-magnetized sedimentary
100 layer and a uniformly and weakly-magnetized crustal layer (0.05 A/m). For crustal thickness (top
101 basement to Moho depth), we used results from both wide-angle data (Shillington et al., 2009)
102 and gravity modelling (Graham et al., 2013). Studies of the Curie temperature (578° C -
103 temperature above which magnetite loses its magnetic properties) in the Black Sea region show
104 that the Curie depth is reached mainly below Moho but sometimes above it, in a depth range of
105 24-36 km (e.g., Starostenko et al., 2014; Aydin et al., 2005; Maden, 2013). Since we are mostly
106 concerned with regions where the Moho is shallower than 24 km, we assumed in this initial
107 model that all the EBSB crust is magnetized.

A crustal magnetization of 0.05 A/m had a limited contribution to the calculated anomaly and the observed anomaly was mostly determined by higher magnetizations near the top of basement. Magnetic modeling is usually performed either assuming a fixed value of magnetization and a variable thickness for the magnetized layer, or a fixed layer thickness and variable magnetization intensities along it (e.g., Banerjee, 1984). In the EBSB, there are no available independent constraints on the thickness or the intensity of magnetic sources. Our strategy was to find a simple model that could be mechanistically justified and was able to simulate the observed magnetic anomaly (Fig. DR2-DR7). We limited the magnetizations to values representative of felsic to mafic igneous rocks (0.2-5.0 A/m; e.g., Hunt et al., 1995) and assumed a constant-thickness magnetized layer subdivided into bands/blocks of variable magnetization, with its top coinciding with the seismically-inferred basement. This type of approach is common, particularly at rifted continental margins (e.g., Banerjee, 1984; Bronner et al., 2011; Collier et al., 2017). In oceanic domains, magnetic layer thicknesses of 0.5 km (e.g., Hussenoeder et al., 1996; Searle et al., 2010), 1.0 km (e.g., Ozima et al., 1974; Searle et al., 1998), 1.5 km (e.g., Bronner et al., 2011), or 2.0 km (e.g., Collier et al., 2017) are generally used. Changes in magnetized layer thickness will affect the intensity of the magnetization inferred (almost inversely proportional to thickness), but will change little the overall trend of the modeled anomaly (e.g., Parker and Huestis, 1974). In this study, we exclude thin magnetized layers of a few hundred meters that would require anomalously high magnetizations to model the observed anomaly. We use a 1 km-thick layer in the oceanic domain because it is consistent with similar work elsewhere and allows us to generate a model with reasonable magnetizations.

Since no independent constraints are available on the thickness of the magnetized layer over the structural highs (Shatsky Ridge and MBSH), and because these areas are only modeled to

provide lateral constraints for the central basin magnetic model, we decided to keep the same constant layer thickness in order to generate a simple and consistent model along the profiles. Volcanic bodies imaged in seismic reflection data (e.g., Nikishin et al., 2003, 2015), and high-density bodies interpreted from gravity modelling (e.g., Starostenko et al., 2004), helped to constrain the distribution of these magnetized bodies and those along the basin margins during the main rifting phase. Based on these assumptions, we updated the starting model to fit adequately the observed field.

Magnetic Anomaly Filtering

A low-pass filter was applied to the calculated anomaly to remove wavelengths shorter than a specified cut-off, thus removing the result of a short-wavelength crustal anomalies such as those caused by local variations of the top basement horizon picked along seismic profiles. We chose a low-pass wavelength cut-off of 25 km. This cut-off allows us to remove some short-period oscillations from the calculated anomaly without removing lateral variations that fall within the wavelength of the observed anomaly. A cut-off > 25 km was observed to remove information resolved by the magnetic anomaly grid (Fig. DR8).

Method Limitations and Data Dependency

The non-uniqueness of the potential field problem requires introducing assumptions such as simplification of geometry, limits to size or depth, and range limits on susceptibility/magnetization values (Paterson and Reeves, 1985). Interpretation of magnetic anomaly may be ambiguous, as any given anomaly could be caused by several possible sources. For example, the amplitude and shape of an anomaly produced by a large body at great depth can

be similar to that of a small body closer to the surface. Changes in depth, shape, and position of the top basement horizon picked from seismic profiles and used as top boundary for the model creation can also affect the resulting calculated anomaly. In addition, attempting to model gridded magnetic data in 2D neglects the fact that the observed data could be affected by features that are out of the plane of the modeled section (3D effects) that make fitting these data very difficult at some locations (e.g., Rippington et al., 2015).

Despite all its limitations, 2D forward magnetic anomaly modeling can provide a quantitative perspective to features visible on seismic data and aid the interpretation in areas where seismic imaging is difficult. The non-uniqueness of the magnetic problem can be reduced in several ways. For example, having an even distribution of seismic lines across the area helps ensuring that any interpretation made on either the seismic or magnetic datasets can be calibrated to and constrained by the other. By interpreting features that fit both independent datasets we can increase the confidence in that interpretation. Also, geological knowledge and literature information is required to produce a reasonable set of modelling parameters.

Here magnetic anomaly modelling allows us to estimate regional scale variations in the magnetization character of crustal elements without specifically correlating small wavelength anomalies to a precise causative body. Although any conclusion inferred from magnetic modelling is strongly model dependent, because of the ambiguity in crustal affinity at the center of the EBSB shown by seismic reflection and refraction data, our magnetic modelling results provide additional and effective insights into crustal affinity and distribution in the center of the EBSB.

REFERENCES

Aydın, İ., Karat, H. İ., and Koçak, A., 2005, Curie-point depth map of Turkey. Geophysical Journal International, 162(2), 633-640. https://doi.org/10.1111/j.1365-246X.2005.02617.x

Banerjee, S. K., 1984, The magnetic layer of the ocean crust—How thick is it?. Tectonophysics, 105(1-4), 15-27. https://doi.org/10.1016/0040-1951(84)90191-4

Baranov, V., 1957, A new method for interpretation of aeromagnetic maps: pseudo-gravimetric anomalies. Geophysics, 22(2), 359-382. https://doi.org/10.1190/1.1438369

Bronner, A., Sauter, D., Manatschal, G., Péron-Pinvidic, G., and Munschy, M., 2011, Magmatic breakup as an explanation for magnetic anomalies at magma-poor rifted margins. Nature Geoscience, 4(8), 549-553. DOI: 10.1038/NGEO1201

Collier, J. S., McDermott, C., Warner, G., Gyori, N., Schnabel, M., McDermott, K., and Horn, B. W., 2017, New constraints on the age and style of continental breakup in the South Atlantic from magnetic anomaly data. Earth and Planetary Science Letters, 477, 27-40. https://doi.org/10.1016/j.epsl.2017.08.007

Graham, R., Kaymakci, N., and Horn, B. W., 2013, The Black Sea: something different. Geo Expro, 10(5), 57-62.

Hippolyte, J. C., Müller, C., Kaymakci, N., and Sangu, E., 2010, Dating of the Black Sea Basin: new nannoplankton ages from its inverted margin in the Central Pontides (Turkey). Geological Society, London, Special Publications, 340(1), 113-136. https://doi.org/10.1144/SP340.7

Hunt, C. P., Moskowitz, B. M., and Banerjee, S. K., 1995, Magnetic properties of rocks and minerals. Rock physics & phase relations: a handbook of physical constants, 3, 189-204. https://doi.org/10.1029/RF003p0189

198 Hussenoeder, S. A., Tivey, M. A., Schouten, H., and Searle, R. C., 1996, Near- bottom magnetic
199 survey of the Mid- Atlantic Ridge axis, 24°–24° 40′ N: Implications for crustal accretion at
200 slow spreading ridges. Journal of Geophysical Research: Solid Earth, 101(B10), 22051-
201 22069. https://doi.org/10.1029/96JB01890
202 Maden, N., 2013, Geothermal structure of the eastern Black Sea basin and the eastern Pontides
203 orogenic belt: Implications for subduction polarity of Tethys oceanic lithosphere.
204 Geoscience Frontiers, 4(4), 389-398. https://doi.org/10.1016/j.gsf.2013.02.001
205 Maus, S., et al., 2009, EMAG2: A 2–arc min resolution Earth Magnetic Anomaly Grid compiled
206 from satellite, airborne, and marine magnetic measurements. Geochemistry, Geophysics,
207 Geosystems, 10(8). doi:10.1029/2009GC002471
208 Meyer, B., Saltus, R., and Chulliat, A., 2017, EMAG2: Earth Magnetic Anomaly Grid (2-arc-
209 minute resolution) Version 3. National Centers for Environmental Information, NOAA.
210 Model. doi:10.7289/V5H70CVX
211 Monteleone, V., Minshull, T. A., and Marin-Moreno, H., 2019, Spatial and temporal evolution of
212 rifting and continental breakup in the Eastern Black Sea Basin revealed by long-offset
213 seismic reflection data, Tectonics, 38, 2646-2667. doi: 10.1029/2019TC005523.
214 Nikishin, A. M., Korotaev, M. V., Ershov, A. V., and Brunet, M. F., 2003, The Black Sea basin:
215 tectonic history and Neogene–Quaternary rapid subsidence modelling. Sedimentary
216 Geology, 156(1-4), 149-168. https://doi.org/10.1016/S0037-0738(02)00286-5
217 Nikishin, A. M., Okay, A. I., Tüysüz, O., Demirer, A., Amelin, N., and Petrov, E., 2015, The
218 Black Sea basins structure and history: New model based on new deep penetration regional
219 seismic data. Part 1: Basins structure and fill. Marine and Petroleum Geology, 59, 638-655.
220 https://doi.org/10.1016/j.marpetgeo.2014.08.017

Ozima, M., Joshima, M., and Kinosmta, H., 1974, Magnetic properties of submarine basalts and the implications on the structure of the oceanic crust. Journal of geomagnetism and geoelectricity, 26(3), 335-354. https://doi.org/10.5636/jgg.26.335

Parker, R. L., and Huestis, S. P., 1974, The inversion of magnetic anomalies in the presence of topography. Journal of Geophysical Research, 79(11), 1587-1593. https://doi.org/10.1029/JB079i011p01587

Paterson, N. R., and Reeves, C. V., 1985, Applications of gravity and magnetic surveys: The state-of-the-art in 1985. Geophysics, 50(12), 2558-2594. https://doi.org/10.1190/1.1441884

Rippington, S., Mazur, S., and Warner, J., 2015, The crustal architecture of the Faroe–Shetland Basin: insights from a newly merged gravity and magnetic dataset. Geological Society, London, Special Publications, 421(1), 169-196. https://doi.org/10.1144/SP421.10

Russell, S. M., and Whitmarsh, R. B., 2003, Magmatism at the west Iberia non-volcanic rifted continental margin: evidence from analyses of magnetic anomalies. Geophysical Journal International, 154(3), 706-730. https://doi.org/10.1046/j.1365-246X.2003.01999.x

Rangin, C., Bader, A. G., Pascal, G., Ecevitoğlu, B., and Görür, N., 2002, Deep structure of the Mid Black Sea High (offshore Turkey) imaged by multi-channel seismic survey (BLACKSIS cruise) 1, 2. Marine Geology, 182(3-4), 265-278. https://doi.org/10.1016/S0025-3227(01)00236-5

Ross, D. A., 1978, Summary of results of Black Sea drilling. Initial Reports of the Deep Sea Drilling Project, 42(Part 2).

Searle, R. C., Cowie, P. A., Mitchell, N. C., Allerton, S., MacLeod, C. J., Escartin, J., Russell, S. M., Slootweg, P. A. and Tanaka, T., 1998, Fault structure and detailed evolution of a slow

spreading ridge segment: The Mid-Atlantic Ridge at 29 N. Earth and Planetary Science Letters, 154(1-4), 167-183. https://doi.org/10.1016/S0012-821X(97)00160-X

Searle, R. C., Murton, B. J., Achenbach, K., LeBas, T., Tivey, M., Yeo, I., et al., 2010, Structure and development of an axial volcanic ridge: Mid-Atlantic Ridge, 45 N. Earth and Planetary Science Letters, 299(1-2), 228-241. https://doi.org/10.1016/j.epsl.2010.09.003

Shillington, D. J., Scott, C. L., Minshull, T. A., Edwards, R. A., Brown, P. J., and White, N., 2009, Abrupt transition from magma-starved to magma-rich rifting in the eastern Black Sea. Geology, 37(1), 7-10. doi: 10.1130/G25302A

Starostenko, V. I., Dolmaz, M. N., Kutas, R. I., Rusakov, O. M., Oksum, E., Hisarli, Z. M., Okyar, M., Kalyoncuoglu, U. Y., Tununsatar, H. E. and Legostaeva, O. V., 2014, Thermal structure of the crust in the Black Sea: comparative analysis of magnetic and heat flow data. Marine Geophysical Research, 35(4), 345-359. doi: 10.1007/s11001-014-9224-x

Starostenko, V., Buryanov, V., Makarenko, I., Rusakov, O., Stephenson, R., Nikishin, A., Georgiev, M., Dimitriu, R., Legostaeva, O., Pchelarov, V. and Sava, C., 2004, Topography of the crust–mantle boundary beneath the Black Sea Basin. Tectonophysics, 381(1-4), 211-233. https://doi.org/10.1016/j.tecto.2002.08.001

Thébault, E., et al., 2015, International geomagnetic reference field: the 12th generation. Earth, Planets and Space, 67(1), 79. DOI 10.1186/s40623-015-0228-9

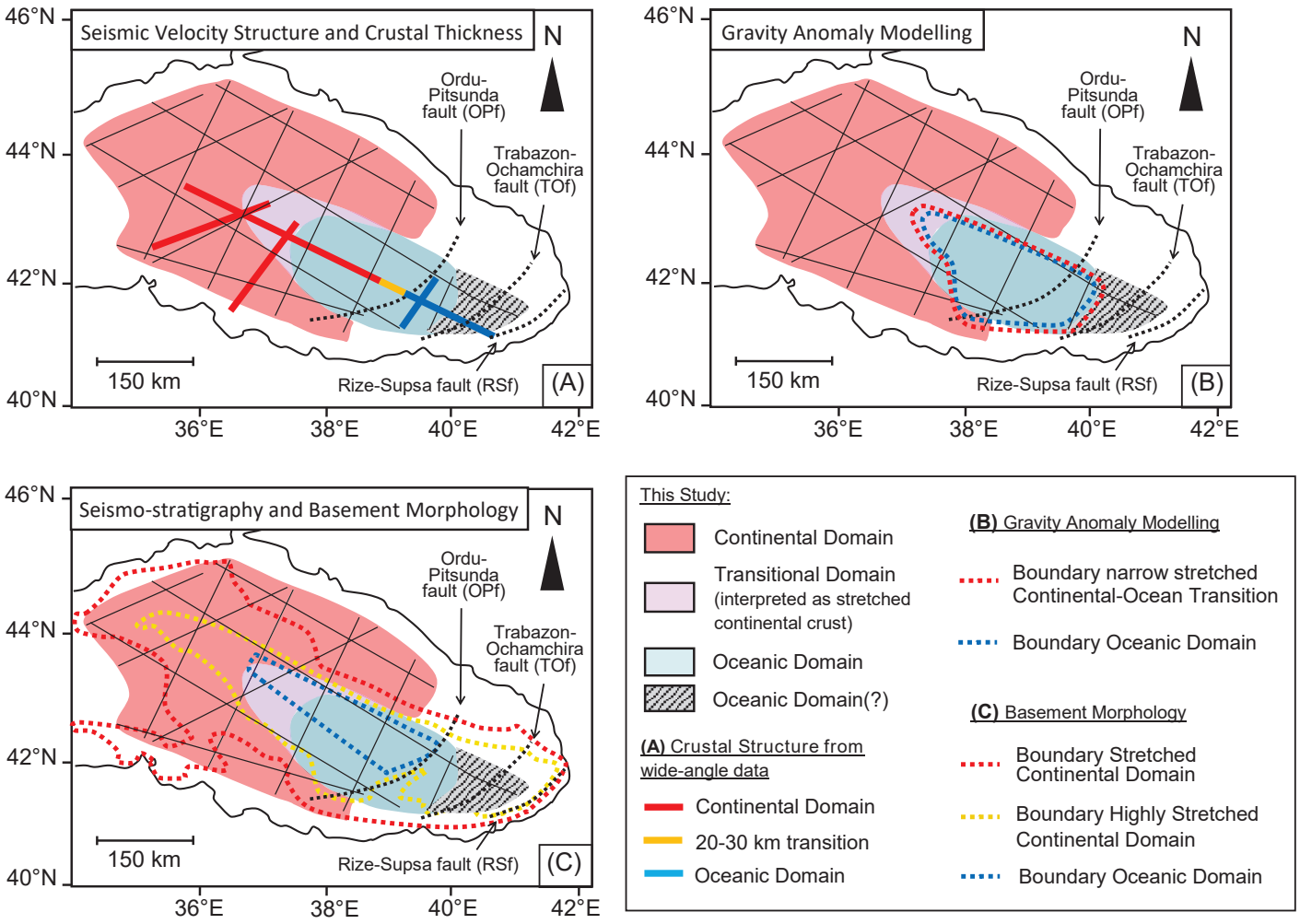

Figure DR1. Comparison between crustal domains boundaries inferred in this study and crustal distribution from other studies using: (A) crustal thickness and lower crustal velocities from wide-angle seismic data (Shillington et al., 2009); (B) gravity anomaly modelling constrained by 2D long-offset seismic reflection profiles (Graham et al., 2013); (C) 2D long-offset seismic reflection profiles interpretation (Nikishin et al., 2015). Note that the extent of oceanic and transitional domains, and the nature of the transition, varies from study to study. In (A), an abrupt, 20-30 km transition from stretched continental to thick oceanic crust is attributed to an along-axis change from magma-poor to magma-rich margin (Shillington et al., 2009); in (B), an extremely abrupt transition zone surrounds the interpreted oceanic domain, and is associated to a ribbon of continental crust intruded by magmatic rocks (Graham et al., 2013); in (C), a wide area of highly-stretched continental crust constitutes the transition to a narrow and elongated, NW-SE-trending oceanic domain (Nikishin et al., 2015). Background colors and colors used to plot crustal distribution/boundaries are explained in the legend.

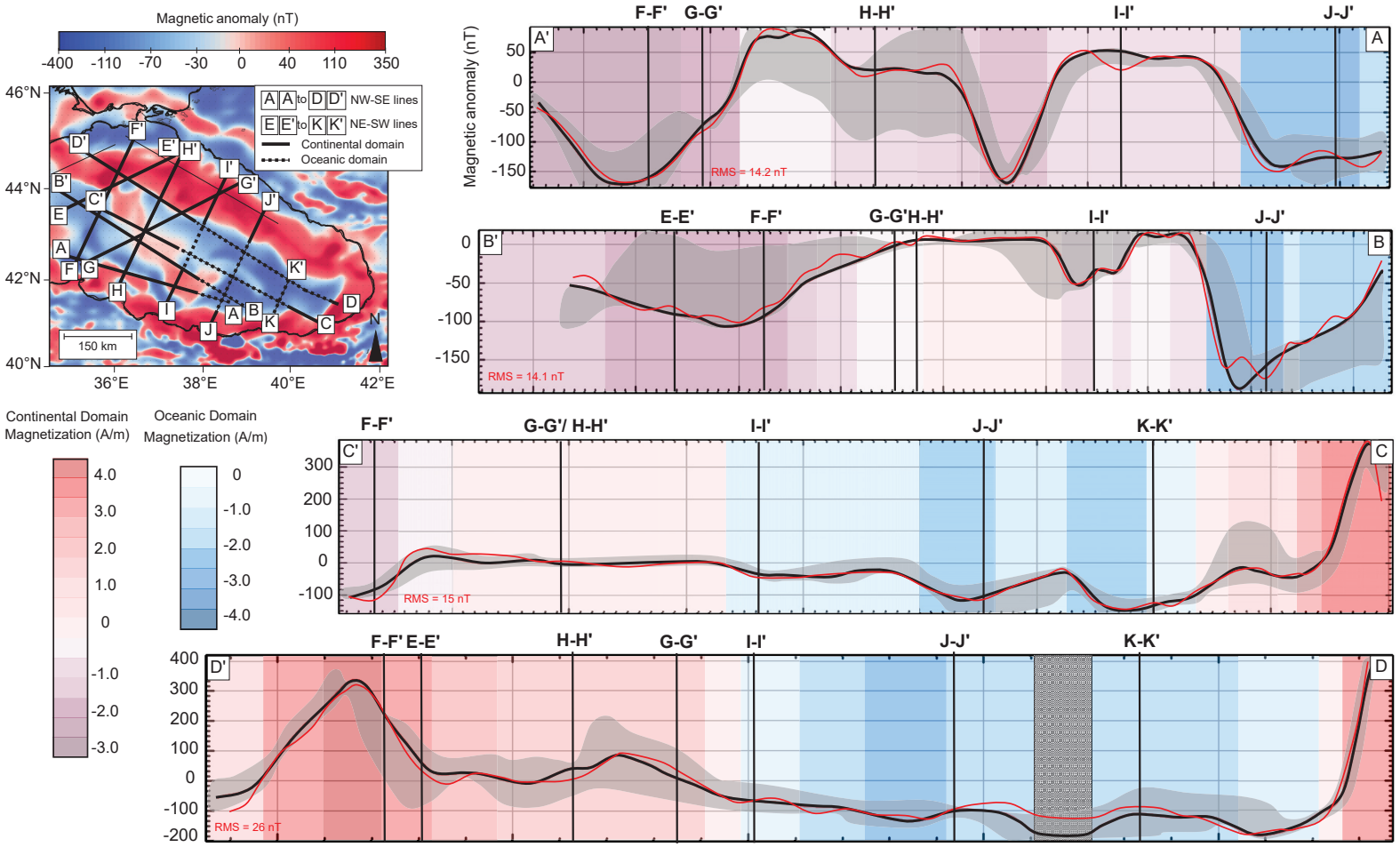

Figure DR2. Magnetic anomaly models along each relevant seismic profile. On the top left corner, the magnetic anomaly map for the EBSB region (RTP EMAG2-v3), with seismic profiles in overlay: thick black lines are modelled profiles where continental crust has been interpreted; thick dotted lines are modelled profiles where oceanic crust has been interpreted. Profiles from A to D are NW-SE trending lines, whereas profiles from E to K are NE-SW trending lines. Each panel compares the calculated (red line) and observed (black line) anomalies. The grey band along the observed anomaly represents the anomaly variations about 15 km either side of the profile. The root mean-squared (RMS) error, expressed in nT, between observed and calculated anomaly is shown at the bottom left corner of each panel. Colored backgrounds along displayed profiles show magnetization intensities for the positively magnetized continental layers (pink), negatively magnetized continental layers (purple), and negatively magnetized oceanic layers (blue). Black vertical lines within each panel show profile intersections. The striped shading over the D-D' profile indicates a gap along the BS-180 seismic line.

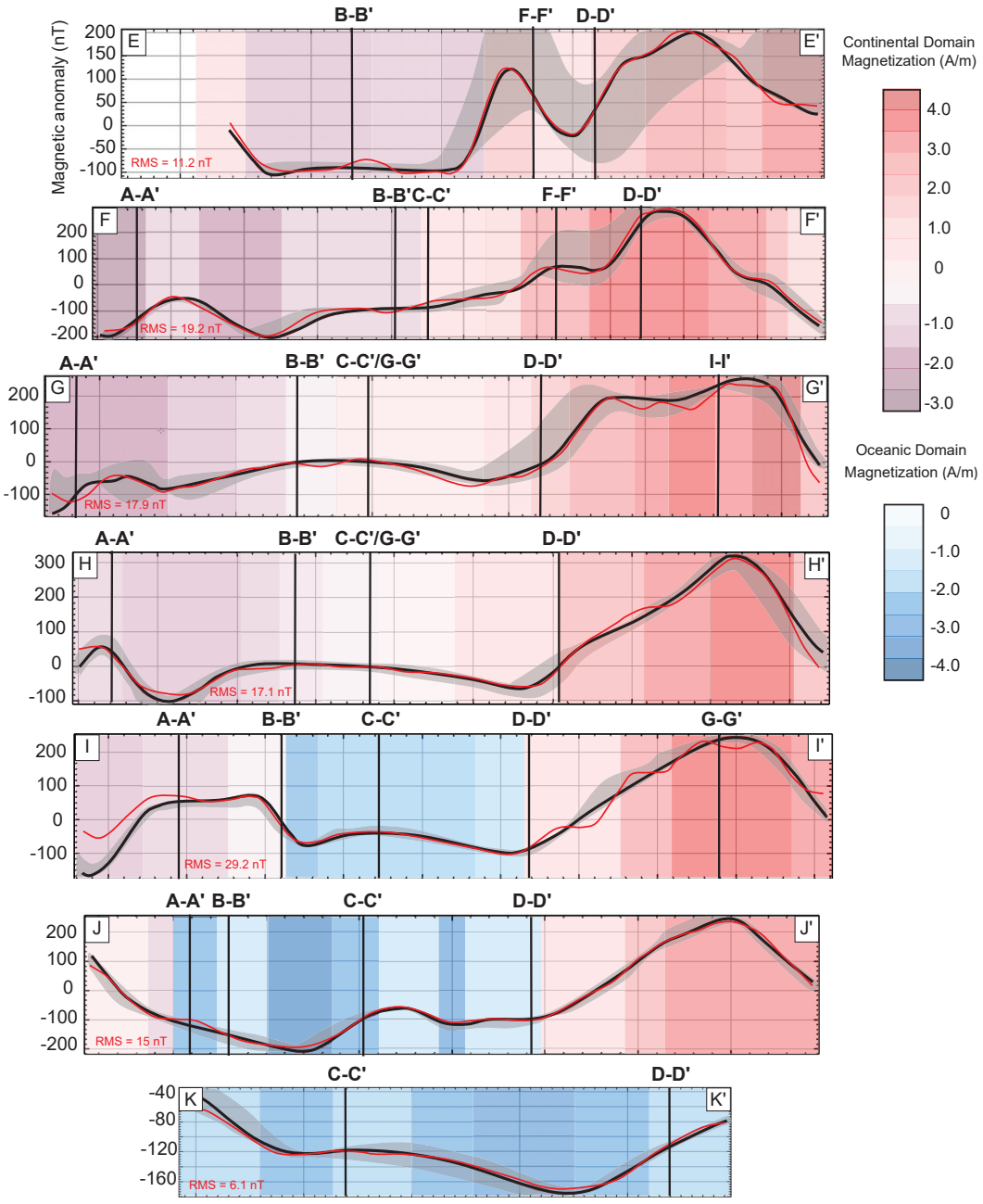

Figure DR2. Continued..

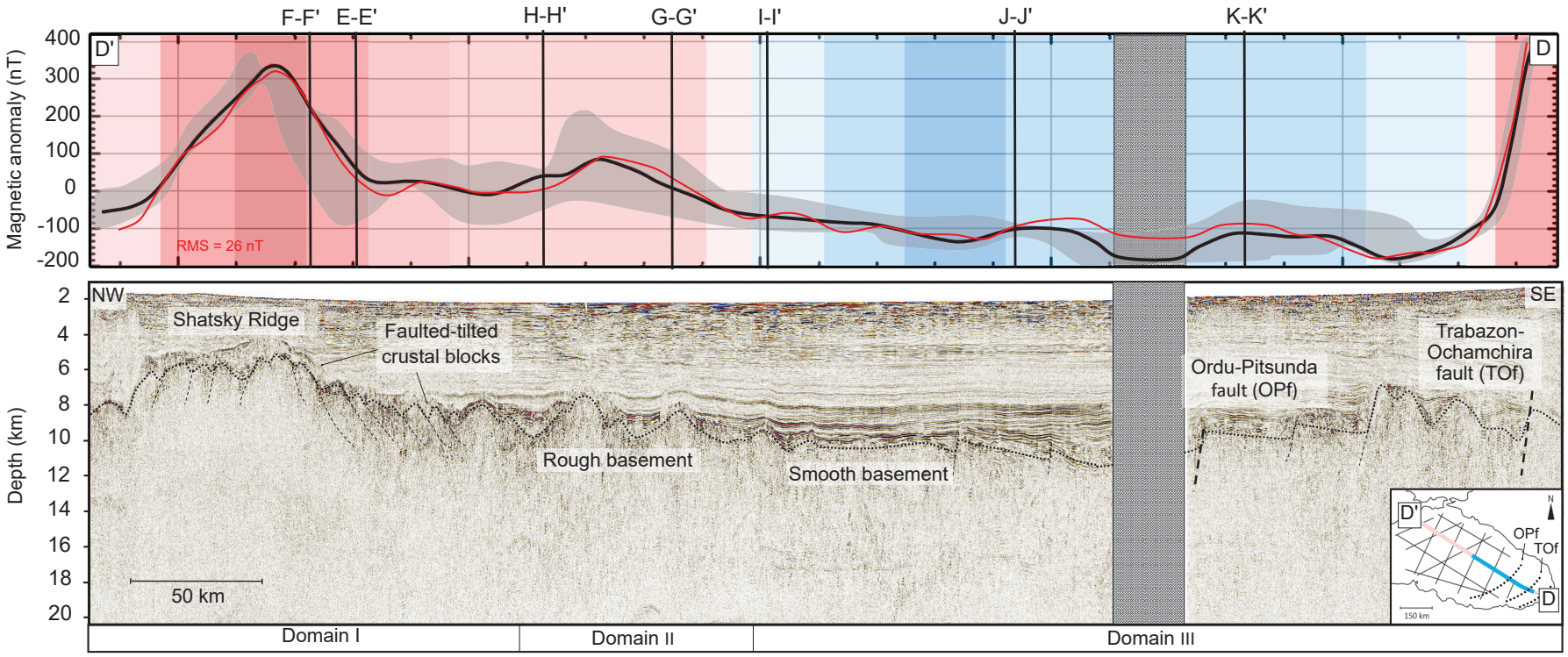

Figure DR3. Magnetic anomaly modelling along seismic profile BS-180. Top panel (Fig. DR2 - D-D') shows the observed (black) and calculated (red) anomaly along this profile. Magnetic intensity is indicated with colored bands (color scale as shown in Fig. DR2). Bottom panel shows the BS-180 seismic profile. Top basement and fault systems interpreted are in overlay. This profile shows the transition from the tilted and faulted blocks of the stretched continental domain (Domain I), to the rough, non-faulted continental basement (Domain II), to the smooth oceanic basement affected by trans-tensional faults (Domain III). The striped shading over the two panels indicates a gap along the seismic profile. The location map at the bottom right corner shows the profile position, with colors associated to the interpreted continental (pink) and oceanic (blue) domains. Trans-tensional faults locations are also shown in the location map (OPf and TOf). (VE = 7)

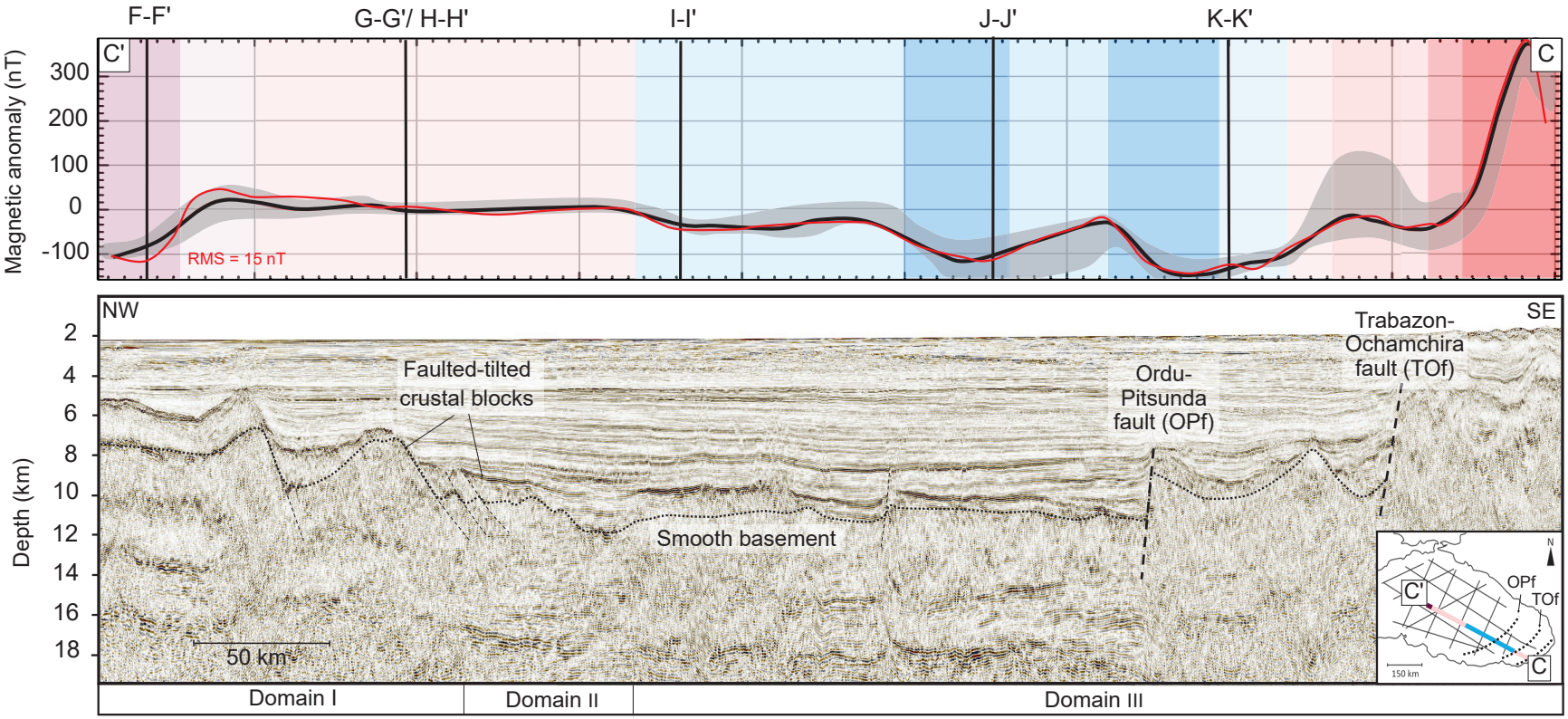

Figure DR4. Magnetic anomaly modelling along seismic profile bp-91-109. Top panel (Fig. DR2 - C-C') shows the observed (black) and calculated (red) anomaly along this profile. Magnetic intensity is indicated with colored bands (color scale as shown in Fig. DR2). Bottom panel shows bp-91-109 seismic profile. Top basement and fault systems interpreted are in overlay. The location map at the bottom right corner shows the profile position, with colors associated to the interpreted continental (pink-purple) and oceanic (blue) domains. Trans-tensional fault locations are also shown in the location map (OPf and TOf). (VE = 7).

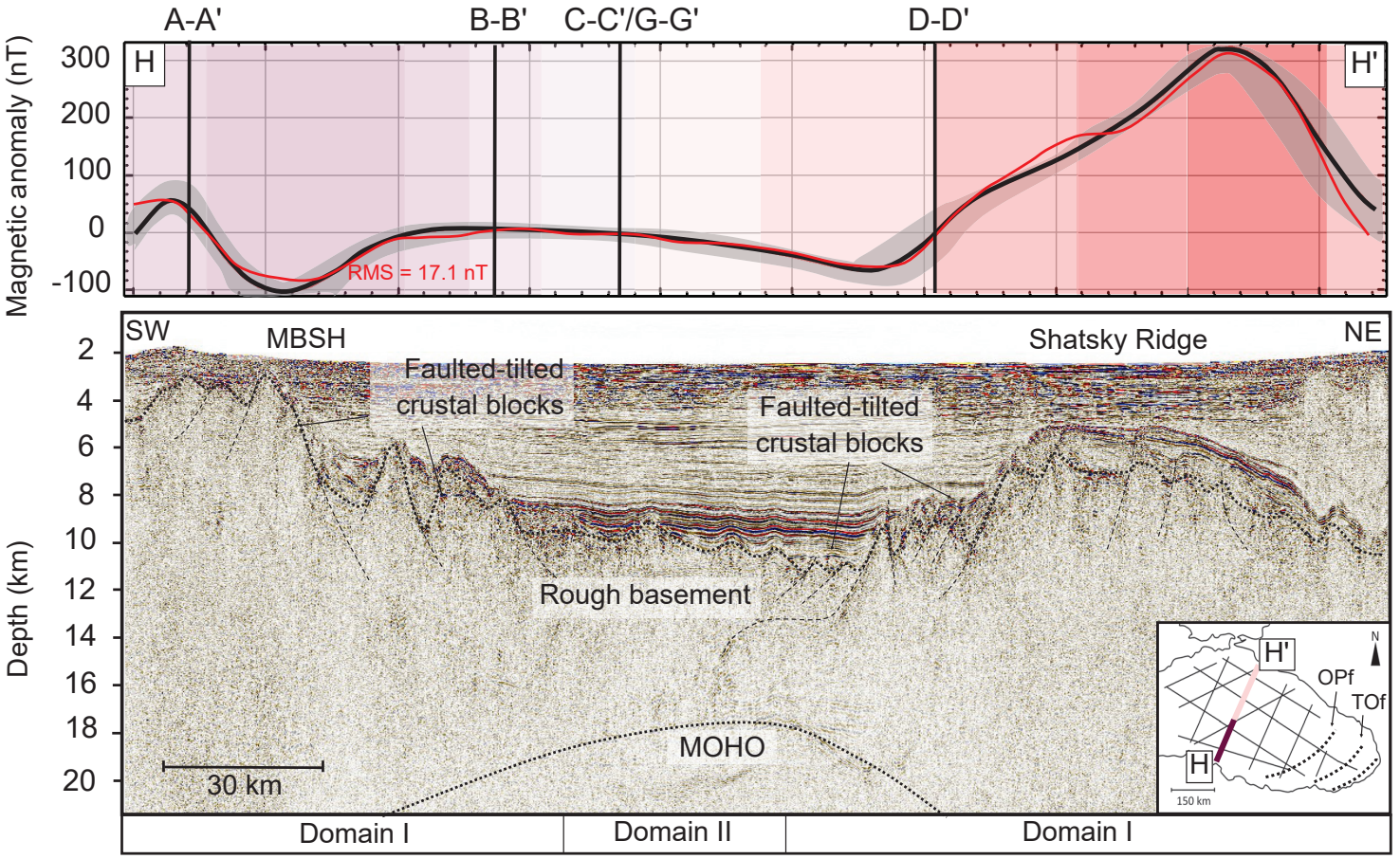

Figure DR5. Magnetic anomaly modelling along seismic profile BS-90. Top panel (Fig. DR2 - H-H') shows the observed (black) and calculated (red) anomaly along this profile. Magnetic intensity is indicated with colored bands (color scale as shown in Fig. DR2). Bottom panel shows the BS-90 seismic profile. Top basement and fault systems interpreted are in overlay. Moho depth comes from Graham et al. (2013) gravity modelling. No oceanic crust is inferred in the central basin (Domain II), where a rough basement is instead associated with stretched continental crust based on the presence of weakly-magnetized layers. The location map at the bottom right corner shows the profile position, with colors marking the interpreted continental (pink-purple) domain. Trans-tensional fault locations are also shown in the location map (OPf and TOf). (VE = 5)

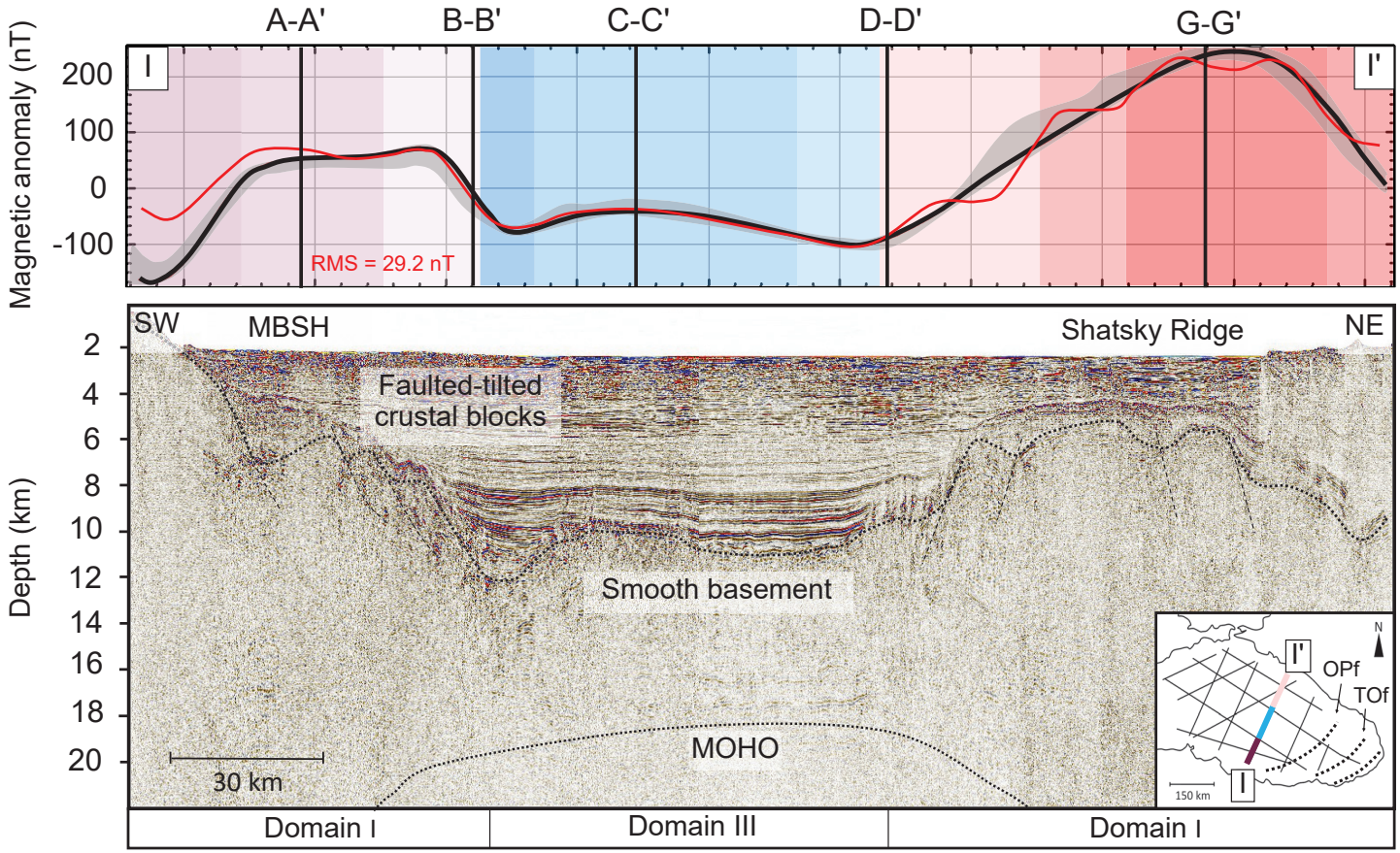

Figure DR6. Magnetic anomaly modelling along seismic profile BS-100. Top panel (Fig. DR2 - I-I') shows the observed (black) and calculated (red) anomaly along this profile. Magnetic intensity is indicated with colored bands (color scale as shown in Fig. DR2). Bottom panel shows the BS-100 seismic profile. Top basement and fault systems are interpreted in overlay. Moho depth comes from Graham et al. (2013) gravity modelling. Domain III is interpreted as an oceanic type of crust, due to its smooth morphology and the strong and negative magnetization character, with intensity between 1.6 and 2.4 A/m. The location map at the bottom right corner shows the profile position, with colors marking the interpreted continental (pink-purple) and oceanic (blue) domains. Trans-tensional fault locations are also shown in the location map (OPf and TOf). (VE = 5)

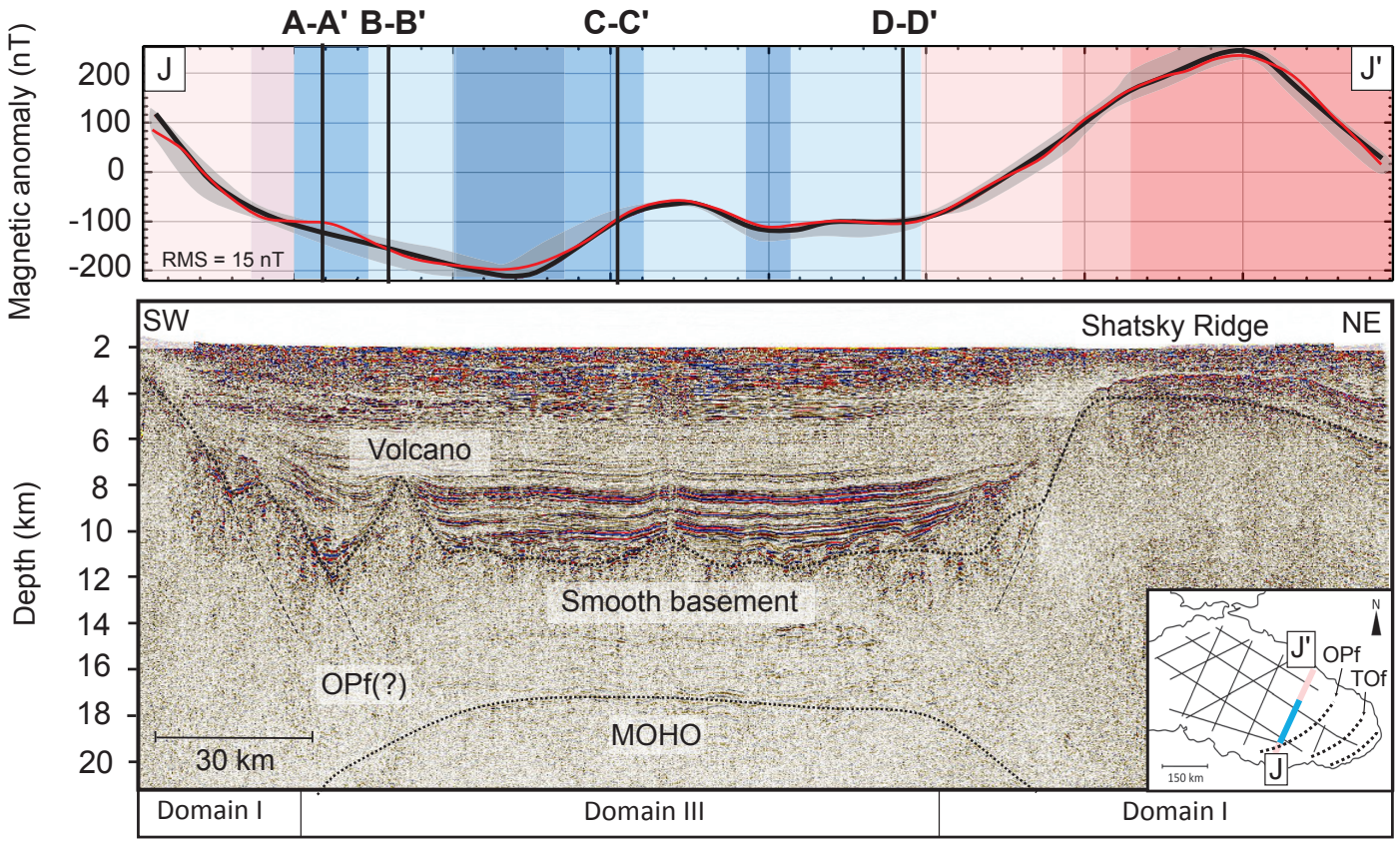

Figure DR7. Magnetic anomaly modelling along seismic profile BS-110. Top panel (Fig. DR2 - J-J') shows the observed (black) and calculated (red) anomaly along this profile. Magnetic intensity is indicated with colored bands (color scale as shown in Fig. DR2). Bottom panel shows the BS-110 seismic profile. Top basement and fault systems are interpreted in overlay. Moho depth comes from Graham et al. (2013) gravity modelling. Domain III is interpreted as oceanic crust, due to its smooth morphology and the strong and negative magnetization character, with intensity between 1.1 and 3.8 A/m. The location map at the bottom right corner shows the profile position, with colors marking the interpreted continental (pink-purple) and oceanic (blue) domains. Trans-tensional fault locations are also shown in the location map (OPf and TOf). (VE = 5)

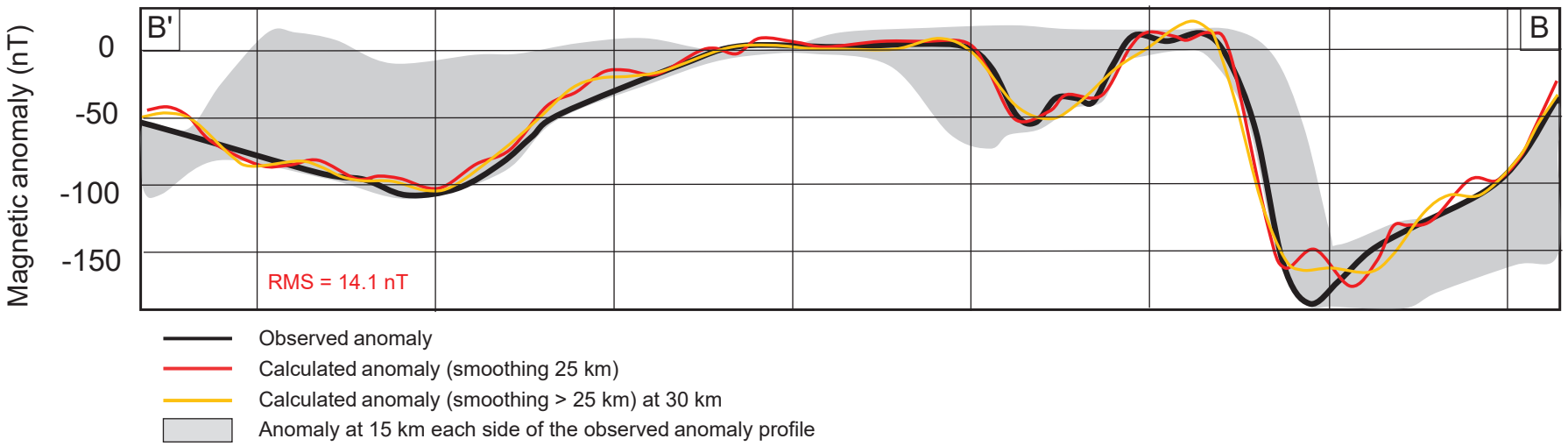

Figure DR8. Magnetic anomaly modelling along seismic profile BS-170 (Fig. DR2 - B-B'). A smoothing > 25 km over the calculated anomaly removes some of the features resolved by the observed anomaly.